IOP Publishing Nanotechnology
Nanotechnology **25** (2014) 195601 (11pp) doi:10.1088/0957-4484/25/19/195601

Micelle-templated composite quantum dots for super-resolution imaging

Jianquan Xu[1], Qirui Fan[1], Kalpesh D Mahajan[1], Gang Ruan[1,2], Andrew Herrington[3], Kayvan F Tehrani[3], Peter Kner[3] and Jessica O Winter[1,4]

[1] William G. Lowrie Department of Chemical and Biomolecular Engineering, The Ohio State University, Columbus, Ohio 43210, USA
[2] Department of Biomedical Engineering, College of Modern Engineering and Applied Sciences, Nanjing University, People's Republic of China
[3] College of Engineering, University of Georgia, Athens, Georgia 30602, USA
[4] Department of Biomedical Engineering, The Ohio State University, Columbus, Ohio 43210, USA

E-mail: winter.63@osu.edu

Received 13 December 2013, revised 15 March 2014
Accepted for publication 18 March 2014
Published 23 April 2014

Abstract

Quantum dots (QDs) have tremendous potential for biomedical imaging, including super-resolution techniques that permit imaging below the diffraction limit. However, most QDs are produced via organic methods, and hence require surface treatment to render them water-soluble for biological applications. Previously, we reported a micelle-templating method that yields nanocomposites containing multiple core/shell ZnS–CdSe QDs within the same nanocarrier, increasing overall particle brightness and virtually eliminating QD blinking. Here, this technique is extended to the encapsulation of Mn-doped ZnSe QDs (Mn–ZnSe QDs), which have potential applications in super-resolution imaging as a result of the introduction of Mn^{2+} dopant energy levels. The size, shape and fluorescence characteristics of these doped QD-micelles were compared to those of micelles created using core/shell ZnS–CdSe QDs (ZnS–CdSe QD-micelles). Additionally, the stability of both types of particles to photo-oxidation was investigated. Compared to commercial QDs, micelle-templated QDs demonstrated superior fluorescence intensity, higher signal-to-noise ratios, and greater stability against photo-oxidization,while reducing blinking. Additionally, the fluorescence of doped QD-micelles could be modulated from a bright 'on' state to a dark 'off' state, with a modulation depth of up to 76%, suggesting the potential of doped QD-micelles for applications in super-resolution imaging.

S Online supplementary data available from stacks.iop.org/nano/25/195601/mmedia

Keywords: quantum dots, doping, superresolution imaging

(Some figures may appear in colour only in the online journal)

1. Introduction

Since their introduction into the biological milieu in 1998, there has been tremendous interest in the application of quantum dots (QDs) for biological imaging [1–5]. In particular, QDs show great promise for super-resolution fluorescence microscopy [6–8], in which fluorescence is localized to a spot size below the diffraction limit by a combination of single molecule imaging and image processing [9–11]. With their high absorbance cross section (approximately an order of magnitude higher than that of typical fluorescent dyes, e.g., $\sim 20 \times 10^{-16}\,cm^2$ for CdSe QDs [12] versus $\sim 1 \times 10^{-16}\,cm^2$ for Kaede [8]) and resistance to photobleaching [1], QDs should permit photons to be collected at a faster rate and for

longer time periods compared to fluorescent dyes and proteins, permitting the same resolution to be attained in less time. QDs have already been employed in super-resolution imaging methods that have used shifts in their emission wavelength upon intentional photo-oxidation [13] and blinking [14, 15] to produce signals below the diffraction limit. With the introduction of photo-switchable Mn-doped ZnSe QDs (Mn–ZnSe QDs) that can be excited at one wavelength while using another wavelength to control the passage of excited electrons down either a fluorescent or non-radiative pathway [16], QDs can potentially be applied in additional super-resolution techniques, such as stimulated emission depletion (STED) microscopy [17]. Giant CdSe/CdS QDs in which the Auger recombination and rapid blinking are strongly suppressed have also been shown to be suitable for STED [18].

However, the majority of QD synthesis methods, including those used to produce Mn–ZnSe [19], require a surface modification step to transfer particles from the organic solution in which they are synthesized to the aqueous phase [20–22]. This is often accomplished via ligand exchange, which can unfortunately result in the deterioration of fluorescence properties, most likely through the introduction or alteration of surface states [23, 24]. In 2002, Dubertret and colleagues [25] introduced a micelle encapsulation process using lipid-polymer amphiphiles to encapsulate single QDs. Recently, we [26, 27] and others [28, 29] have expanded this concept to the encapsulation of multiple nanospecies within a single micelle core. Because nanospecies are encapsulated within the hydrophobic core of the micelle, they may be used as synthesized, with the hydrophilic polymer block providing water solubility. Thus, no surface treatment or ligand exchange is required, and QD-micelles retain their same pre-encapsulation functional properties, while displaying increased brightness and reduced blinking, since there are several QDs in each micelle [27]. Micelle encapsulation can theoretically be used to encapsulate any hydrophobic species smaller than the micelle core and can also be used to co-encapsulate multiple types of nanoparticles, resulting in composites such as magnetic QDs [26, 28, 29] or magnetic-gold nanoparticles [30].

Here, we expand the micelle encapsulation approach to photo-switchable Mn–ZnSe QDs synthesized according to standard organic methods [19], evaluating the size, shape, and fluorescence properties of the resulting micelle nanocomposites and comparing these results to those of commercially-available ZnS–CdSe organic QDs. Additionally, we evaluate the influence of the micelle coating on stability to photo-oxidation, as the micelle coating may provide a method for altering fluorescence properties of QDs synthesized via organic methods. Finally, we demonstrate feasibility of micelle encapsulated doped-QDs for application in STED microscopy.

2. Experimental

2.1. Materials

Zinc stearate (12.5–14%, ZnO), selenium powder (99.999%, ~200 mesh), tetramethylammonium hydroxide pentahydrate (TMAH, 25% w/w in methanol), manganese chloride ($MnCl_2$, 97%), and octadecylamine (ODA, 98%) were purchased from Alfa Aesar. Stearic acid (SA, ⩾98.5%), 1-octadecene (ODE, ⩾95.0%), 3-Mercaptopropionic acid (MPA, ⩾99%), and tributyl phosphine (TBP, 97%), acetone (⩾99.9%), and Poly (vinyl alcohol) (13 000–23 000 Dalton, 87–89% hydrolyzed, PVA) were purchased from Sigma-Aldrich. Chloroform was purchased from Mallinchrodt Chemicals. Poly(styrene-b-ethylene glycol) (PS-PEG) with a molecular weight of 3800-b-6500 (Dalton) was purchased from Polymer Source. Organic ZnS–CdSe QDs ($\lambda_{em} = 605$ nm) in decane and carboxy-ZnS–CdSe QDs ($\lambda_{em} = 605$ nm) in pH 9 borate buffer were purchased from Invitrogen.

2.2. Preparation of the Mn–ZnSe QDs

Mn-doped ZnSe QDs were synthesized according to the method of Peng [19, 21].

2.2.1. Synthesis of $MnSt_2$ precursor. Briefly, 1.42 g of SA was dissolved in 10 mL of methanol in a 100 mL three-neck flask and heated to 50–60 °C until the solution became clear. The solution was then allowed to cool to room temperature. Next, TMAH solution was prepared by adding 2.3 mL of TMAH stock solution to 1.5 mL of methanol. This solution was added dropwise to the SA solution until the white precipitate disappeared. Then, 0.315 g of $MnCl_2$ was dissolved in 3.15 mL of methanol and added dropwise via an addition funnel into the above solution under vigorous stirring, causing a white precipitate to form and flocculate. This precipitate was collected, washed with methanol six times, and dried under vacuum.

2.2.2. Synthesis of Mn–ZnSe QDs. In a typical experiment, TBP–Se stock solution was prepared inside a glove box by adding 0.63 g of Se to 2.7 mL of TBP. One and a half milliliters of this solution was mixed with 1.3 g of ODA in a 25 mL flask, removed from the glove box, immediately protected with Ar, and heated to about 70 °C under Ar. Also, $ZnSt_2$ stock solution was prepared by adding 2.5 g $ZnSt_2$, 0.5 g stearic acid, and 12 mL ODE to a 50 mL flask. The solution was maintained at ~150 °C and degassed with argon.

Then, 25 mL of ODE and 0.1 g of $MnSt_2$ were loaded into a 100 mL three-neck flask, heated to 110 °C, and bubbled under argon for 20 min. The temperature was increased to 280 °C and the argon source changed from bubbling to flow. Once the reaction temperature reached 280 °C, 3 mL of TBP–Se stock solution was swiftly injected. After 5 min, the temperature was reduced to 260 °C and held for 60 min. The temperature of the reaction was then increased to 290 °C, 4 mL of the heated $ZnSt_2$ stock solution was injected into the reaction solution, and 0.6 g ODA in 0.6 mL ODE was heated using a heat gun and injected into the reaction solution. After 15 min, the remainder of the $ZnSt_2$ stock solution was injected into the reaction flask in 3 mL intervals every 15 min for a total of three injections followed by ODE/ODA injection. The reaction solution was next cooled to room temperature, and

the nanocrystals were purified using chloroform and acetone. Briefly, 1 mL of chloroform was added to 1 mL of reaction solution, and heated using a heat-gun until the solution became clear. Two milliliters of acetone was then added to the solution to precipitate the QDs. The nanocrystals were isolated by centrifugation at 4000 rpm for 3 min and dispersed in 1 mL of chloroform for further use. This purification step was repeated three times.

2.3. Synthesis of water-soluble QDs by ligand exchange

Both water-soluble ZnS–CdSe and Mn–ZnSe QDs were produced from organic precursors in chloroform via ligand exchange with 3-mercaptopropionic acid (MPA). Organic ZnS–CdSe QDs in decane were first transferred to chloroform using a methanol/isopropanol mixture (75/25 in volume) to precipitate the QDs, which were then diluted to 0.1 μM for further use. Twenty microliters of MPA were added to100 μL of QDs (either Zn–CdSe or Mn–ZnSe in chloroform), and after vortexing for 20 min, the flocculated MPA-capped QDs were isolated by centrifugation. QDs were washed once with chloroform, and then dispersed in 3 mL of water. $NaHCO_3$ was then added to the solution until the QDs were completely dissolved.

2.4. Synthesis of the QD-encapsulated micelles

Micelles encapsulating QD nanoparticles were created using the interfacial instability process [31]. QDs and PS-PEG co-polymer amphiphile (i.e., 50 μL ZnS–CdSe QDs and 10 μL polymer; 200 μL Mn–ZnSe QDs and 20 μL polymer) were mixed thoroughly in a 1.5 mL centrifuge tube. This mixture was added to an aqueous solution of poly(vinyl alcohol) (800 μl, 5 mg mL^{-1}), which served as a surfactant. After vortexing for 3 min, the emulsion formed was transferred to an open container (i.e., a 10 mL glass vial) to permit evaporation of the chloroform. The vial was rotated to spread emulsion droplets on the wall and to enhance the rapid evaporation of chloroform. The milky emulsion droplets became transparent after the removal of chloroform, indicating the formation of micelles containing QDs.

2.5. Characterization of QDs and QD-micelles

Transmission electron microscopy (TEM) observations were performed using an FEI Tecnai G2 Spirit TEM. To observe micelles, samples were negatively stained with 1% phosphotungstic acid before observation. Absorption spectra were collected with a Thermo Electron Corporation Genesys 6 spectrophotometer. Fluorescence emission spectra were measured using a PTI QuantaMaster™ 40. Quantum yield was determined using commercial ZnS–CdSe QDs in decane (Invitrogen) with known quantum yield (80%) as a reference using a method adapted from Peng [19]. These particles have an overlapping emission peak with that of the Mn–ZnSe QDs and can be excited at the same wavelength. Dynamic fluorescence intensity was measured using an Olympus BX41 microscope (100x oil immersion objective) equipped with a 100 W mercury lamp (Chiu Technical Corporation). Fluorescence emission was filtered through a long-pass filter and collected by a Photometrics Evolve EMCCD camera. Fluorescence intensity measurements over time were analyzed using MetaMorph Basic software (Olympus).

2.6. Photo-oxidization and photo-modulation measurements

To perform photo-oxidation and photo-modulation measurements, 15 μl of QD solution was dried on a cover slip, which was then mounted on a glass slide using 3–5 μl of glycerol or ultra-pure distilled water (18.2 MΩ cm). If QDs on the slide were too dense for measurement, lower concentrations slides were attempted. Photo-oxidation measurements were performed on multiple QDs in a defined area (figure S1, available at stacks.iop.org/nano/25/195601/mmedia), with representative data shown. Photo-oxidization data was acquired using an Olympus IX71 inverted microscope with a 60x oil objective (Plan Apo N). The microscope is equipped with a PriorProScan xy stage and a Prior NanoScanZ piezo stage for focusing. Fluorescence was imaged using an Andor EMCCD camera (DV887DCS-BV with 14bit ADC). Between the microscope and the CCD camera, additional optics were inserted including a deformable mirror (Mirao 52E, Imagine Optics) for PSF correction and two lenses for an extra 3x magnification so that the 16 micron CCD pixel size corresponds to 89 nm at the sample. The sources of light used for the tests were a 405 nm LED (Thorlabs M405L2) and a 488 nm Laser (Spectra-Physics 488 nm Cyan Laser System). The LED light was set to 119 μW for continuous exposure and the laser source was set to 20 mW. In the non-continuous tests, the sample was exposed to 100 ms of light exposure on each step. Each step of the test was repeated at a range of z levels to track the location of the QDs during movement.

To measure the modulation of Mn–ZnSe QDs, the QDs were excited with widefield excitation from the 405 nm LED and imaged on the Andor Camera as above. The excitation intensity was less than 1 W cm^{-2}. To modulate the QDs, the slide was additionally excited with a focused spot from a 660 nm laser (100 mW, OBIS 660 LX, Coherent), which served as the modulation beam. The modulation spot was created by slightly under-filling the back aperture of the microscope objective and was focused onto the image plane. The spot diameter was 1.0 μm full width at half maximum. The intensity of the modulation beam at the sample could be varied up to 12.5 MW cm^{-2}.

Data from these experiments was analyzed using ImageJ software. The software recognizes fluorescent spots (i.e., QDs) in each frame and can track QD movement to a new position. The mean value of emission intensity of each QD was measured; values are normalized to their initial intensity. For each test, measurements were performed on several QDs, and in cases demonstrating the same pattern, the series with highest intensity (hence the least noise) was chosen for comparison.

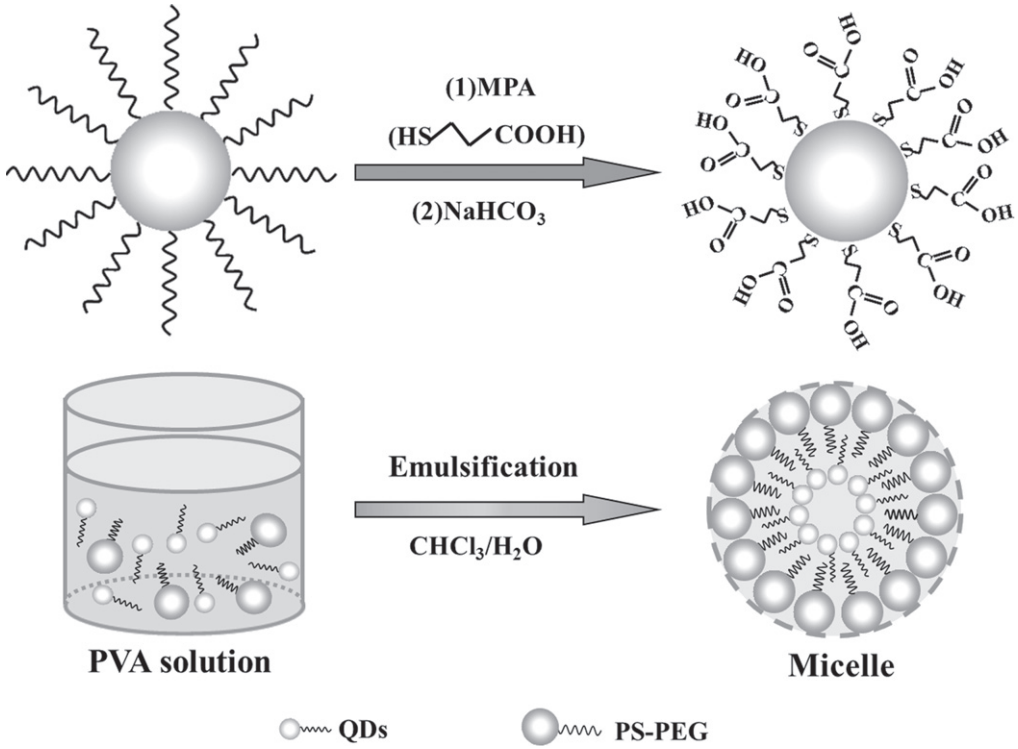

Figure 1. Schematic of the ligand exchange process (top) and micelle-templated assembly of ZnS–CdSe QDs and Mn–ZnSe QDs (bottom).

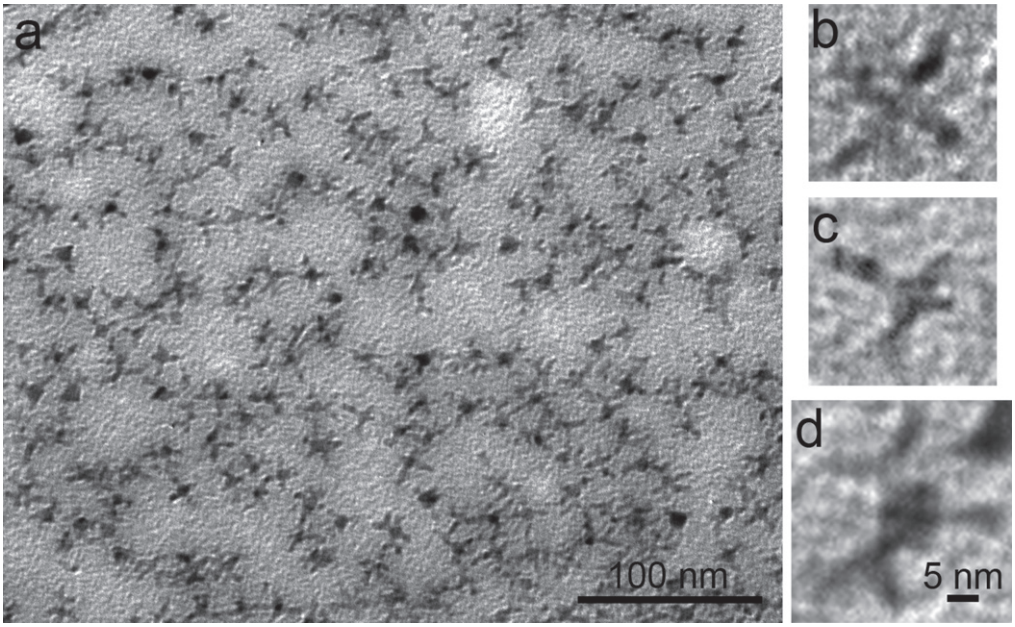

Figure 2. (a) Mn-doped ZnSe QDs. Particles adopt a tetrapod appearance (b), (c), which can include arm branching (d).

3. Results and discussion

3.1. QD synthesis

To compare the efficacy of micelle encapsulation to standard water-solubilization methods, ZnS–CdSe and Mn–ZnSe QDs were prepared using either ligand exchange or micelle encapsulation (figure 1). In both cases, organic QDs were used as precursors. For the ligand exchange approach, the original organic layer (i.e., either trioctylphosphine oxide, TOPO, or ODA for ZnS–CdSe and Mn–ZnSe, respectively) was replaced with hydrophilic carboxyl groups using mercaptopropionic acid as the ligand exchange reagent [21]. Similarly, micelle particles were obtained via the interfacial instability route [31] by evaporating chloroform solvent in the presence of particles and amphiphile in an aqueous emulsion.

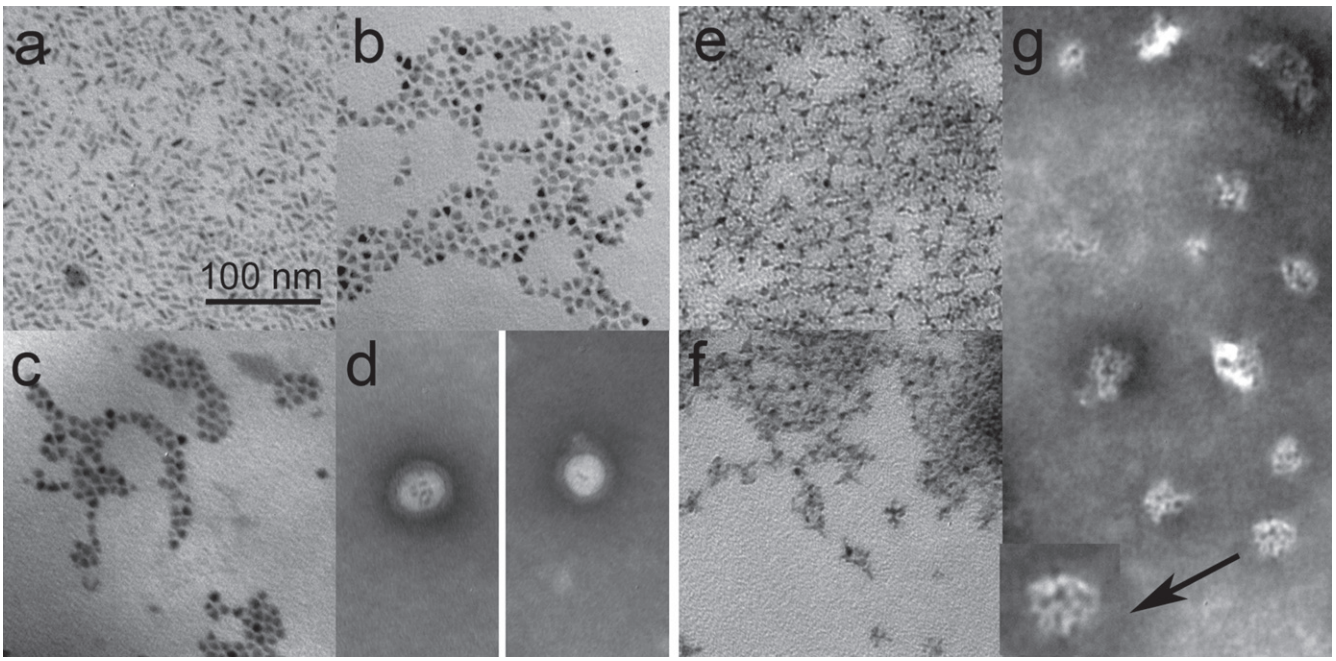

Figure 3. TEM images of the particles. (a)–(d) ZnS–CdSe QDs. (a) Organic QDs, (b) commercial, water-soluble QDs, (c) water-soluble QDs generated through ligand exchange, (d) two examples of micelles formed from organic QDs; (e)–(g) Mn–ZnSe QDs. (e) organic QDs, (f) water-soluble QDs generated through ligand exchange, (g) micelles. Inset shows the micelle indicated by the black arrow at 2X increased magnification. Scale bar = 100 nm for all images except inset.

3.2. QD size and morphology

Interestingly, the morphology of Mn–ZnSe QDs differs from that of traditional core/shell particles (figures 2, 3(e) versus figure 3(a)), which display a spherical or elongated oblong appearance. Mn-doped ZnSe QDs demonstrate a tetrapod shape, which has been reported previously for other semiconductor QD materials [32–35], but, to our knowledge, not for Mn–ZnSe QDs. This is in contrast to previous reports that indicated the formation of spherical QDs using a similar synthesis procedure [19, 21]. Nanostructure formation generally proceeds in two steps: nucleation and growth, which can occur simultaneously in the same solution. Several factors influence the rates of these processes, including ratio of transition metal (e.g., Mn, Zn) to chalcogen (e.g., S, Se, Te), synthesis temperature, and the presence of impurities, including capping ligands, in solution. For tetrapods to form, anisotropic growth must occur. Usually, this results from the growth of one material phase (e.g., wurtzite) favored under certain synthesis conditions on a nucleated particle of a different material phase (e.g., zinc-blende) that was formed under different synthesis conditions. For example, CdTe tetrapods are initially nucleated with a zinc-blende structure containing four facets upon which growth of a nearly-lattice matched wurtzite structure can occur, yielding four arms, and therefore, tetrapod formation [32]. It is likely that Mn–ZnSe tetrapod synthesis begins with MnSe nucleation in the zinc-blende phase, as reported previously for spherical Mn–ZnSe nanoparticles [19], followed by growth of ZnSe arms in the wurtzite phase. Anisotropic growth is influenced by many factors, including the reactant ratio. Increasing the transition metal to chalcogen ratio favors growth over nucleation, enhancing anisotropic growth and tetrapod arm length [32]. In addition, selection of capping ligand is a strong influence on anisotropic growth, often favoring growth in a specific crystal plane, as shown by oleylamine-induced enhancement of growth in the [0001] direction in CdTe tetrapods [34] and the roles of phosphonic acid and hexadecylamine in the synthesis of CdTe [32] and CdS [35] tetrapods, respectively. In this work, a higher concentration of the additional zinc monomer was employed compared to the initially reported synthesis procedure [19]. This resulted in a higher Zn:Se ratio, which is most likely responsible for the observed Mn–ZnSe tetrapod structure; although, the higher concentration of ODA employed could also play a role. Also, some tetrapods show branched arms (figure 2(d)), as has been reported previously for other structures [33]. Generally, arms will continue linear growth if the material remains in the wurtzite phase; however, if zinc blende layers or stacking faults are present near the end of arms, a dendritic structure will emerge from the initial arms [32].

The average diameter of commercial, ZnS–CdSe QDs was determined to be ~8 nm, as indicated by TEM observations (figures 3(b), (c)), and ~6 nm for Mn–ZnSe QDs (figures 3(e), (f)), consistent with previous reports [19]. It should be noted that organic ZnS–CdSe QDs displayed an elongated morphology (figure 3(a)), but became spherical after the ligand exchange (figure 3(c)). This might be caused by intraparticle ripening, which has been reported previously for these nanocrystals [36] and gold nanoparticles [37, 38]. Both types of particles (e.g., ZnS–CdSe QDs and Mn–ZnSe QDs) were incorporated into micelles, and several QDs were evident in each micelle (figures 3(d), (g)). Micelle size was ~40 nm for ZnS–CdSe particles (figure 3(d)) and ~30–50 nm

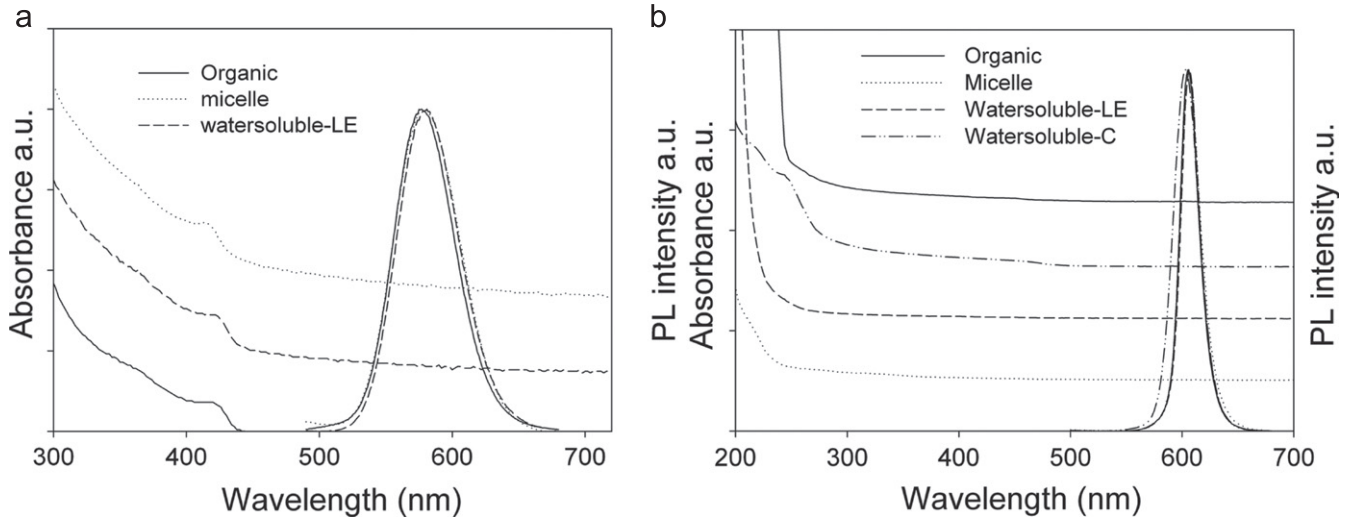

Figure 4. Absorption and fluorescence spectra of (a) Mn–ZnSe-based and (b) ZnS–CdSe based particles.

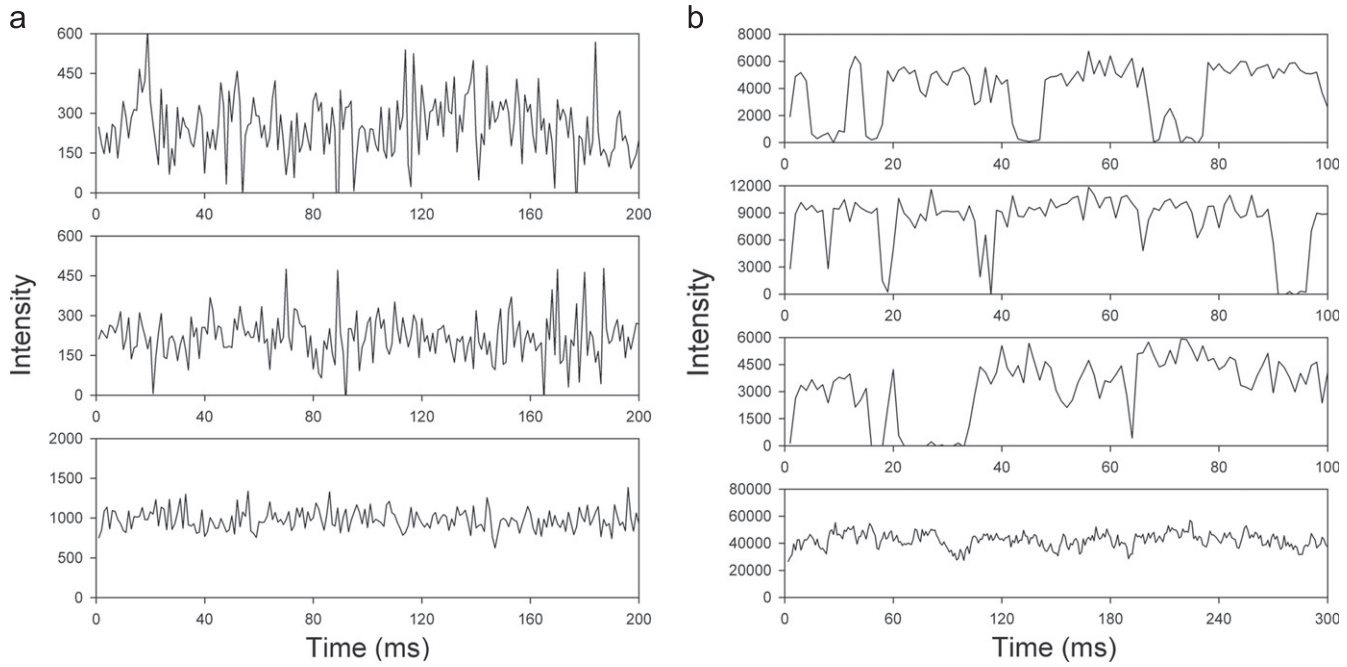

Figure 5. Fluorescence intensity for single QDs and QD micelles. (a) Mn–ZnSe-based particles. From top to bottom: organic QDs, water-soluble QDs made by ligand exchange, and micelles. (b) ZnS–CdSe-based particles. From top to bottom: organic QDs, commercial water-soluble QDs, water-soluble QDs made by ligand exchange, and micelles.

for Mn–ZnSe particles (figure 3(g)). Compared to micelles encapsulating ZnS–CdSe QDs, those encapsulating Mn–ZnSe display an irregular shape, most likely resulting from the irregular shape of the tetrapod encapsulants. It is interesting to note that despite this irregularity, encapsulation is still possible. This result is consistent with reports of encapsulation of rod shaped-QDs in similar micelles [26, 28].

3.3. QD optical properties

To evaluate the effect of micellarization on QD optical properties, micelle-encapsulated Mn–ZnSe QDs (micelle) were compared to particles in the organic phase (organic) and to particles produced via ligand exchange with MPA (water-soluble-LE) (figure 4(a)). Mn–ZnSe micelle particles displayed similar spectral properties to organic and ligand exchange QDs, including both absorption and emission spectra. The quantum yield of micelle-encapsulated Mn–ZnSe QDs was 26%, lower than that of the original organic QDs (40.7%) and QDs produced via ligand exchange with MPA (42.1%).

For comparison, commercial organic CdSe–ZnS QDs were also modified using ligand exchange with MPA and micelle encapsulation to render them water-soluble (organic, water-soluble-LE, and micelle, respectively) and compared to commercially-available water-soluble QDs (water-soluble-C)

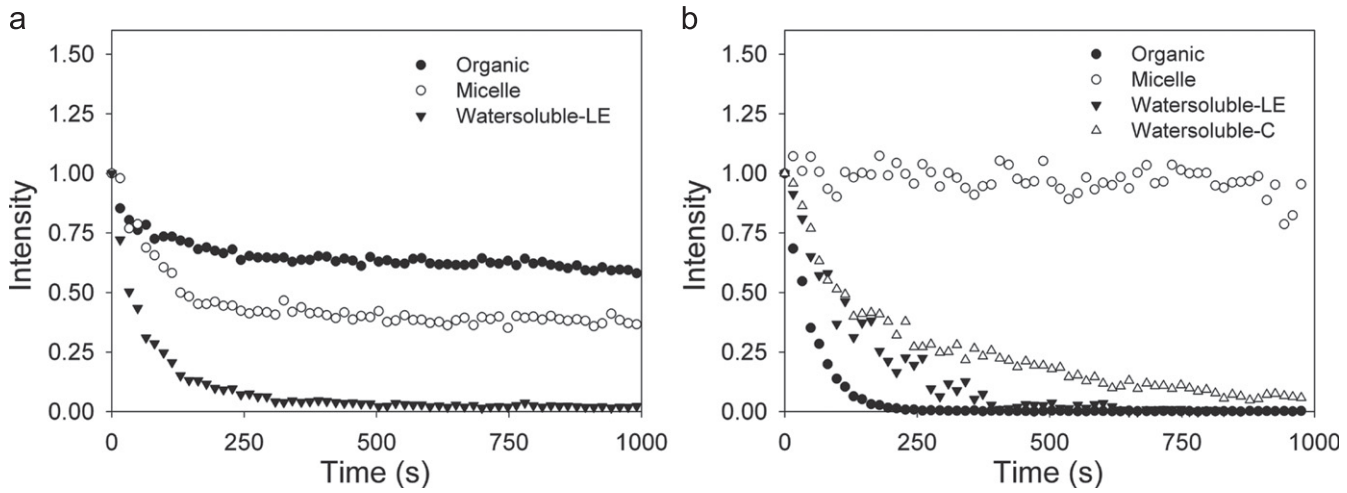

Figure 6. Photo-oxidization measurement. Each curve is normalized to the relative intensity at 0 s. (a) Relative intensity of Mn–ZnSe QD micelles continuously exposed to excitation light of 405 nm. (b) Relative intensity of CdSe–ZnS QDs and micelles continuously exposed to excitation light of 405 nm.

(figure 4(b)). In all cases, virtually no difference between the spectra was seen, indicating that the ligand exchange and micellarization processes do not dramatically change QD absorbance and emission wavelengths. The quantum yield of the micelle-encapsulated CdSe–ZnS QDs was 26.4%, equivalent to that obtained for QDs produced via ligand-exchange QDs (25.3%), but lower than that of the original, organic QDs dissolved in chloroform (48.7%) and commercially-available water-soluble QDs (86%).

The loss of quantum yield observed upon micellarization of commercial ZnS–CdSe QDs most likely results from disruption of the surface ligands, which may change the blinking statistics as a result of changes in the local environment and/or surface traps. A similar loss was observed with the MPA ligand exchange method, consistent with this hypothesis. However, the fluorescence signal of Mn–ZnSe QDs is not believed to originate from trapped or surface states [21], and no loss of quantum yield is observed upon MPA ligand exchange, supporting this theory. Thus, it is likely that the diminution of quantum yield upon micelle encapsulation results from another cause, such as increased particle proximity, which may enhance particle–particle interactions and non-radiative energy transfer, or from the environmental conditions encountered during the micellarization process. However, as many QDs are incorporated in each micelle, micelle QDs still show much higher brightness than single QDs, as described below.

To evaluate fluorescence dynamics, single particle fluorescence intensity of micelle Mn–ZnSe QDs was compared to that of organic and water-soluble QDs produced via ligand exchange (figure 5(a)) as a function of time. For single QDs in both the organic and ligand exchange samples, fluorescence intensity fluctuated between ~0–600 au (average intensity = 249 ± 115 and 218 ± 82 for organic and ligand exchange samples, respectively) with several instances that approached a value of zero, indicating blinking. However, the total fluorescence intensity of micelle particles always remained above zero (ranging between ~600–1400 au) and was ~4X that of individual QDs (average intensity = 979 ± 130).

Similar results were observed for commercially-available ZnS–CdSe micelles encapsulated in micelles when compared to their organic QD precursors and water-soluble QDs produced via ligand exchange and water-soluble QDs sold commercially (figure 5(b)). Single QDs demonstrated variations in fluorescence intensity that resulted in multiple evidences of blinking (fluorescence intensity ranging from ~0–6700, ~0–6000, and ~0–12 000 au for organic, ligand exchange, and commercial QDs, respectively), whereas micelle QDs demonstrate an ~4–13X increase in brightness (42 382 ± 5494 au versus 3786 ± 2137, 3230 ± 1750, and 8714 ± 3043 au for organic, ligand exchange and commercial QDs, respectively) with no evidence of blinking (intensity ranging from ~26 000–57 000 au). The large difference in fluorescence intensity between the two types of samples examined, i.e., ZnS–CdSe and Mn–ZnSe, results from differences in exciton fluorescence lifetime (a few ns for ZnS–CdSe QDs [39] and ~90 μs for Mn–ZnSe QDs [40], and the filter set employed, which was optimized for ZnS–CdSe QDs.

The elimination of blinking behavior is the result of encapsulating multiple QDs within the same micelle core, and thus although individual QDs may lose fluorescence as a result of blinking, the ensemble continues to emit a continuous signal [27]. Increased brightness also results from the aggregation of multiple QDs within a micelle. It should be noted that the micelles reported here are ~40 nm in diameter (figure 3) versus 10–20 nm for commercially-available QDs, and micelle sizes can range from ~10–100 nm in diameter [25, 29]. Thus, this increase in fluorescence comes at the expense of only a marginal increase in nanoparticle size. These enhanced optical properties (i.e., reduced blinking and increased brightness) should significantly improve signal-to-noise ratio in tracking studies.

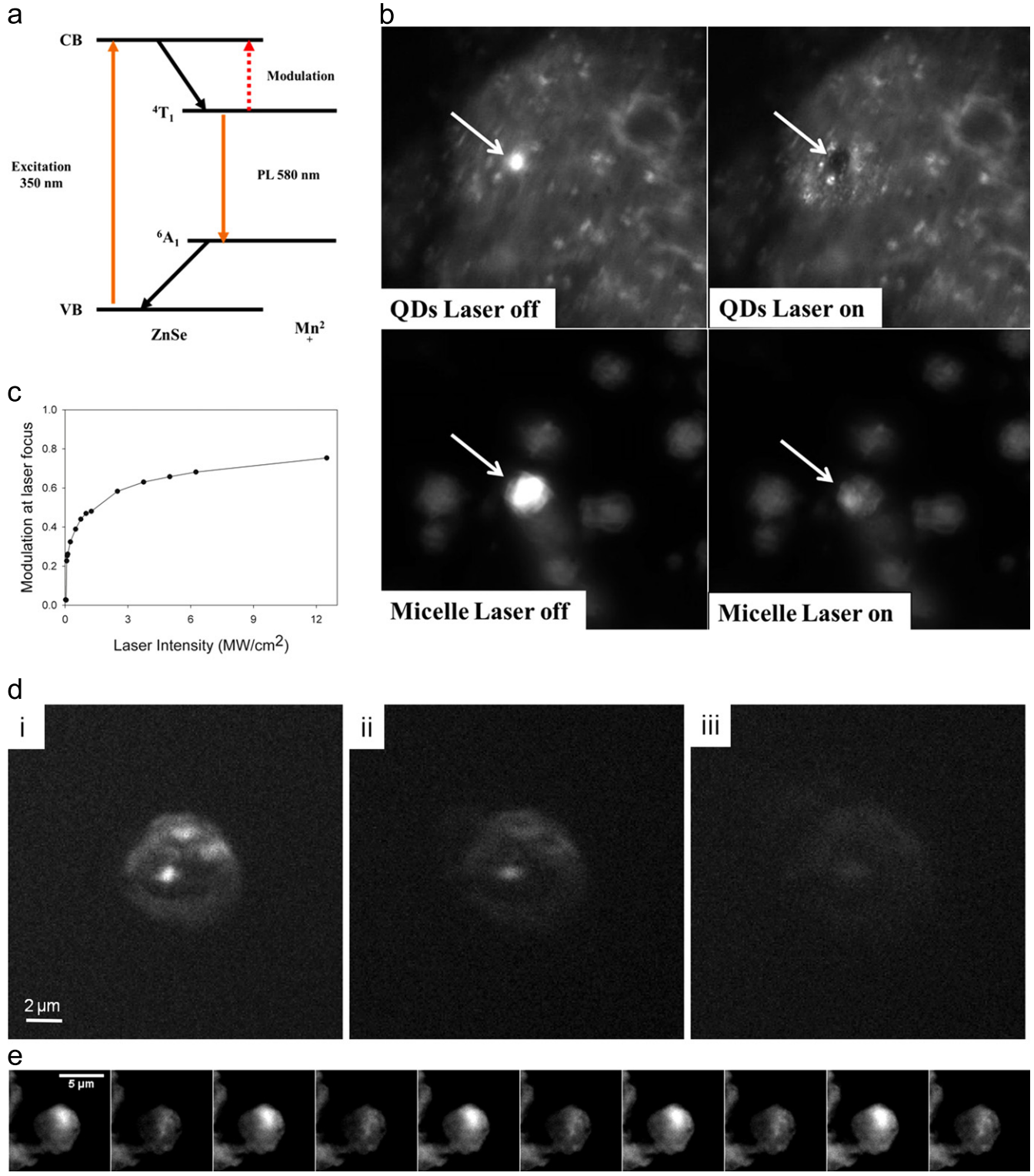

Figure 7. (a) Schematic of the electronic transitions of Mn–ZnSe QDs. (Adapted with permission from [16]. Copyright © 2008 Wiley-VCH.) (b) Fluorescence modulation of Mn–ZnSe QDs (top) and Mn–ZnSe QD micelles (bottom). (c) Modulation depth of Mn–ZnSe QDs as a function of 660 nm laser intensity. The emission is brighter at the focus of the modulating laser because the quantum dots fluoresce brighter when they are first excited. (d) Thin layer films of Mn–ZnSe QDs are excited with a 405 nm LED and modulated with a 660 nm laser (i) 0 MW cm^{-2} modulation intensity, (ii) 0.625 MW cm^{-2} modulation intensity, (iii) 6.25 MW cm^{-2} modulation intensity. (e) Five cycles of modulation of Mn–ZnSe QDs micelles. The micelles are excited with a 365 nm LED, and modulated with a 660 nm laser as described in the methods. The modulation depth is 0.55 ± 0.02 and does not diminish over the course of the measurement.

3.4. QD stability to photo-oxidation

An important consideration for QD use in many super-resolution imaging methods is resistance to photo-bleaching, which permits signal to be collected for longer periods of time, increasing image resolution. Resistance to photo-oxidation is also an important consideration in reducing nanoparticle toxicity, as constituent atoms ejected during the oxidation process (e.g., Cd^{2+} for ZnS–CdSe QDs) can produce considerable toxicity in biological applications [41]. To examine the effect of micelle encapsulation on resistance to photo-oxidation, micelle Mn–ZnSe QDs were compared to organic and aqueous QDs produced via ligand exchange (figure 6(a)). QDs were excited continuously using a 405 nm LED with a power of 119 μW. Organic QDs demonstrated best overall performance, maintaining 60–70% of their initial intensity value over the time period investigated (~17 min), whereas water-soluble QDs produced via ligand exchange demonstrated the worst performance, losing 50% of their initial fluorescence intensity value (i.e., I_{50}) in the first 1–2 min of exposure. In contrast, although micelle encapsulated QDs demonstrated an I_{50} of ~2 min, there was very little additional loss of fluorescence over time. Thus, micelle encapsulation significantly improved resistance to photo-oxidation compared to QDs produced via the ligand exchange method, while yielding a water-soluble product suitable for biological imaging applications.

In addition, the resistance to photo-oxidation of ZnS–CdSe QDs in micelles was examined and compared to that of QDs in the organic phase, rendered water-soluble through ligand exchange, and aqueous QDs sold commercially (figure 6(b)). The fluorescence intensity of organic QDs, QDs rendered water-soluble through MPA ligand exchange, and commercially-available water-soluble QDs rapidly declined, with I_{50} values of <2 min. Micelle QDs demonstrated the best overall resistance to photo-bleaching, with no significant loss of fluorescence over the time period investigated (~17 min), although an I_{50} of ~30 min was measured in subsequent testing (figure S2, available at stacks.iop.org/nano/25/195601/mmedia). Resistance to photo-oxidation was dependent on the power and wavelength of incident light. For example, excitation with a 20 mW 488 nm laser source yielded I_{50} values of ~35 min for micelle encapsulated ZnS–CdSe QDs and ~8 min for commercially-available aqueous ZnS–CdSe QDs. In both cases, the QD photo-oxidation rate was also dependent on the light exposure rate. QDs not continuously exposed were significantly more resistant to photo-oxidation (data not shown).

3.5. QD photo-modulation

The fluorescence emission mechanism of doped-QDs has been previously reported, with significant differences from that of traditional core/shell QDs [21]. In doped-QDs, as in core/shell materials, an exciton, consisting of a hole in the valence band and an electron in the ZnSe conduction band, is generated through the absorption of a photon (figure 7(a)). However, unlike core/shell materials, the exciton rapidly transfers its energy to the dopant energy levels of the Mn^{2+} ions ($^4T_1$). At this point there are several possible outcomes. In the absence of additional energy input, the electrons will most likely decay radiatively to the $^6A_1$ state and then return to the ground state, releasing photons. However, if additional energy is added, the electrons can be pumped into higher energy states through excited-state absorption, from which they make radiation-less transitions to the ground state, effectively quenching fluorescence [42].

Mn–ZnSe QDs can generally be excited at wavelengths shorter than 450 nm, yielding an emission peak centered at 580–600 nm (e.g., figure 4(a)). By adding an additional excitation source at a longer wavelength (650–800 nm), fluorescence emission can be suppressed [16], and therefore modulated. The ability of the investigator to control fluorescence signal potentially permits doped QDs to be employed in super-resolution imaging techniques, including STED microscopy [11] and structured illumination microscopy [43].

There is some question as to whether micellarization could influence this process. In micelles, QDs are packed closely together, increasing the opportunity for interactions resulting from proximity. To evaluate this possibility, photo-modulation of unencapsulated Mn–ZnSe QDs was compared to that of QDs encapsulated in micelles (figure 7(b)). In this experiment, QD clusters were excited by a 119 μW 405 nm LED, while a 100 mW 660 nm laser was employed as the modulation beam. When the 660 nm laser was off, QD emission was clearly evidenced in the excitation spot (figure 7(b), white arrows). However, when the 660 nm laser was applied, emission at the laser spot was suppressed, demonstrating the potential for investigator control of QD fluorescence emission. Results were similar whether particles were examined in a thick film (figure 7(b)), as might be expected in super-resolution imaging, or in thin films (figure 7(d)). This response also demonstrated reversibility and little change in modulation depth; even for particles that were several months old (figure 7(e)). The modulation depth of both materials was further investigated and found to be 76% and 79% for micelle encapsulated and doped QDs, respectively (figure 7(c)). From three separate measurements of the modulation depth versus intensity, the modulation depth was found to be 0.72 ± 0.05 for intensities greater than 1.25 MW cm^{-2}. (Modulation is a function of the modulating laser intensity and does not exceed 80% because the layer of QDs in the sample is thicker than the focal volume, so not all QDs in the region are modulated.) The modulation results, figures 7(b) and (e), are taken from a sequence of images in which the modulation laser is alternately turned off then on. QDs that are modulated in this way fluoresce brighter than QDs that are not modulated and continuously fluoresce. QDs are known to fluoresce brighter upon first excitation as a result of either photo-brightening or photo-bleaching. The modulation depth is constant and does not increase or decrease as the modulation laser is cycled on and off, although the absolute brightness of the modulated particles in both the 'on' state and 'off' state is enhanced, most likely as a result of photo-brightening [44]. Thus, micelle encapsulated QDs

demonstrate nearly equivalent modulation depth to unencapsulated QDs, suggesting their potential application in super-resolution imaging applications.

4. Conclusion

Here, we demonstrate the influence of micelle encapsulation, an emerging water solubilization method, on two types of QDs: Mn–ZnSe QDs and core/shell ZnS–CdSe QDs with potential applications in super-resolution imaging. Interestingly, the Mn–ZnSe QDs employed demonstrated a previously unreported tetrapod shape, yet were still capable of being encapsulated via the micelle approach. Micelle encapsulation was shown to have little influence on QD absorbance or emission wavelength. However, micelle QDs displayed a 4–13X increase in brightness compared to organic QDs and QDs produced via ligand exchange as a result of the micelle aggregation effect [27]. Additionally, micelle QDs demonstrated no observable blinking behavior, an important consideration for single particle tracking experiments. Micellarization was also shown to enhance resistance to photo-oxidation compared to other water solubilization methods, while not interfering with modulation depth. Additionally, micellarization is compatible with a wide range of QDs, including giant CdSe/CdS QDs, which have also been demonstrated for us in STED [18]. The potential for increased photon collection over a longer time period with QD micellarization should enhance image resolution compared to that obtained with QDs produced via ligand exchange. The combination of increased resistance to photo-oxidation and increased brightness makes micelle QDs attractive candidates for super-resolution imaging applications.

Acknowledgments

The authors gratefully acknowledge the support of the National Science Foundation MCB-1052623. In addition, the authors acknowledge the support of Carol Lynn Alpert, Museum of Science Boston, for contributions to manuscript editing. GR and JOW are equity holders of Core Quantum Technologies (CQT), a company commercializing quantum dots for pathological imaging. CQT provided no funding or services for this work.

References

[1] Chan W C and Nie S 1998 Quantum dot bioconjugates for ultrasensitive nonisotopic detection *Science* **281** 2016–8
[2] Goldman E R, Balighian E D, Mattoussi H, Kuno M K, Mauro J M, Tran P T and Anderson G P 2002 Avidin: a natural bridge for quantum dot-antibody conjugates *J. Am. Chem. Soc.* **124** 6378–82
[3] Nagy A, Steinbrück A, Gao J, Doggett N, Hollingsworth J A and Iyer R 2012 Comprehensive analysis of the effects of CdSe quantum dot size, surface charge, and functionalization on primary human lung cells *ACS Nano* **6** 4748–62
[4] Bruchez M, Moronne M, Gin P, Weiss S and Alivisatos A P 1998 Semiconductor nanocrystals as fluorescent biological labels *Science* **281** 2013–6
[5] Mattoussi H, Palui G and Na H B 2012 Luminescent quantum dots as platforms for probing *in vitro* and *in vivo* biological processes *Adv. Drug Delivery Rev.* **64** 138–66
[6] Huang B 2010 Super-resolution optical microscopy: multiple choices *Curr. Opin. Chem. Biol.* **14** 10–4
[7] Patterson G H 2009 Fluorescence microscopy below the diffraction limit *Semin. Cell Dev. Biol.* **20** 886–93
[8] Fernández-Suárez M and Ting A Y 2008 Fluorescent probes for superresolution imaging in living cells *Nat. Rev. Mol. Cell Biol.* **9** 929–43
[9] Rust M J, Bates M and Zhuang X W 2006 Sub-diffraction-limit imaging by stochastic optical reconstruction microscopy (STORM) *Nat. Methods* **3** 793–5
[10] Betzig E, Patterson G H, Sougrat R, Lindwasser O W, Olenych S, Bonifacino J S, Davidson M W, Lippincott-Schwartz J and Hess H F 2006 Imaging intracellular fluorescent proteins at nanometer resolution *Science* **313** 1642–5
[11] Hell S W and Wichmann J 1994 Breaking the diffraction resolution limit by stimulated-emission stimulated-emission-depletion fluorescence microscopy *Opt. Lett.* **19** 780–2
[12] Leatherdale C A, Woo W-K, Mikulec F V and Bawendi M G 2002 On the absorption cross section of CdSe nanocrystal quantum dots *J. Phys. Chem.* B **106** 7619–22
[13] Hoyer P, Staudt T, Engelhardt J and Hell S W 2011 Quantum dot blueing and blinking enables fluorescence nanoscopy *Nano Lett.* **11** 245–50
[14] Lidke K A, Rieger B, Jovin T M and Heintzmann R 2005 Superresolution by localization of quantum dots using blinking statistics *Opt. Express* **13** 7052–62
[15] Dertinger T, Colyer R, Iyer G, Weiss S and Enderlein J 2009 Fast, background-free, 3D super-resolution optical fluctuation imaging (SOFI) *Proc. Natl Acad. Sci. USA* **106** 22287–92
[16] Irvine S E, Staudt T, Rittweger E, Engelhardt J and Hell S W 2008 Direct light-driven modulation of luminescence from Mn-doped ZnSe quantum dots *Angew. Chem. Int. Ed.* **47** 2685–8
[17] Hell S W 2007 Far-field optical nanoscopy *Science* **316** 1153–8
[18] Lesoine M D, Bhattacharjee U, Guo Y J, Vela J, Petrich J W and Smith E A 2013 Subdiffraction, luminescence-depletion imaging of isolated, giant, CdSe/CdS nanocrystal quantum dots *J. Phys. Chem.* C **117** 3662–7
[19] Pradhan N and Peng X G 2007 Efficient and color-tunable Mn-doped ZnSe nanocrystal emitters: control of optical performance via greener synthetic chemistry *J. Am. Chem. Soc.* **129** 3339–47
[20] Smith A M, Duan H W, Rhyner M N, Ruan G and Nie S M 2006 A systematic examination of surface coatings on the optical and chemical properties of semiconductor quantum dots *Phys. Chem. Chem. Phys.* **8** 3895–903
[21] Pradhan N, Battaglia D M, Liu Y C and Peng X G 2007 Efficient, stable, small, and water-soluble doped ZnSe nanocrystal emitters as non-cadmium biomedical labels *Nano Lett.* **7** 312–7
[22] Zhang Y and Clapp A 2011 Overview of stabilizing ligands for biocompatible quantum dot nanocrystals *Sensors* **11** 11036–55
[23] Kloepfer J A, Bradforth S E and Nadeau J L 2005 Photophysical properties of biologically compatible CdSe quantum dot structures *J. Phys. Chem.* B **109** 9996–10003
[24] Aldana J, Wang Y A and Peng X 2001 Photochemical instability of CdSe nanocrystals coated by hydrophilic thiols *J. Am. Chem. Soc.* **123** 8844–50

[25] Dubertret B, Skourides P, Norris D J, Noireaux V, Brivanlou A H and Libchaber A 2002 *In vivo* imaging of quantum dots encapsulated in phospholipid micelles *Science* **298** 1759–62
[26] Ruan G, Vieira G, Henighan T, Chen A R, Thakur D, Sooryakumar R and Winter J O 2010 Simultaneous magnetic manipulation and fluorescent tracking of multiple individual hybrid nanostructures *Nano Lett.* **10** 2220–4
[27] Ruan G and Winter J O 2011 Alternating-color quantum dot nanocomposites for particle tracking *Nano Lett.* **11** 941–5
[28] Park J H, von Maltzahn G, Ruoslahti E, Bhatia S N and Sailor M J 2008 Micellar hybrid nanoparticles for simultaneous magnetofluorescent imaging and drug delivery *Angew. Chem. Int. Ed. Engl.* **47** 7284–8
[29] Bae J, Lawrence J, Miesch C, Ribbe A, Li W K, Emrick T, Zhu J T and Hayward R C 2012 Multifunctional nanoparticle-loaded spherical and wormlike micelles formed by interfacial instabilities *Adv. Mater.* **24** 2735–41
[30] Kim B-S and Taton T A 2006 Multicomponent nanoparticles via self-assembly with cross-linked block copolymer surfactants *Langmuir* **23** 2198–202
[31] Zhu J T and Hayward R C 2008 Spontaneous generation of amphiphilic block copolymer micelles with multiple morphologies through interfacial instabilities *J. Am. Chem. Soc.* **130** 7496–502
[32] Manna L, Milliron D J, Meisel A, Scher E C and Alivisatos A P 2003 Controlled growth of tetrapod-branched inorganic nanocrystals *Nat. Mater.* **2** 382–5
[33] Manna L, Scher E C and Alivisatos A P 2000 Synthesis of soluble and processable rod-, arrow-, teardrop-, and tetrapod-shaped CdSe nanocrystals *J. Am. Chem. Soc.* **122** 12700–6
[34] Xie R G, Kolb U and Basche T 2006 Design and synthesis of colloidal nanocrystal heterostructures with tetrapod morphology *Small* **2** 1454–7
[35] Jun Y W, Lee S M, Kang N J and Cheon J 2001 Controlled synthesis of multi-armed CdS nanorod architectures using monosurfactant system *J. Am. Chem. Soc.* **123** 5150–1
[36] Peng Z A and Peng X 2001 Mechanisms of the shape evolution of CdSe nanocrystals *J. Am. Chem. Soc.* **123** 1389–95
[37] Ji X H, Song X N, Li J, Bai Y B, Yang W S and Peng X G 2007 Size control of gold nanocrystals in citrate reduction: the third role of citrate *J. Am. Chem. Soc.* **129** 13939–48
[38] Zhao L, Ji X, Sun X, Li J, Yang W and Peng X 2009 Formation and stability of gold nanoflowers by the seeding approach: the effect of intraparticle ripening *J. Phys. Chem.* C **113** 16645–51
[39] Cooper D R, Suffern D, Carlini L, Clarke S J, Parbhoo R, Bradforth S E and Nadeau J L 2009 Photoenhancement of lifetimes in CdSe/ZnS and CdTe quantum dot-dopamine conjugates *Phys. Chem. Chem. Phys.* **11** 4298–310
[40] Hell S W, Irvine S E, Staudt T, Rittweger E and Engelhardt J 2008 Direct light-driven modulation of luminescence from Mn-doped ZnSe quantum dots *Angew. Chem. Int. Ed.* **47** 2685–8
[41] Kotov N A *et al* 2009 Nanomaterials for neural interfaces *Adv. Mater.* **21** 3970–4004
[42] Chen H Y, Chen T Y, Berdugo E, Park Y, Lovering K and Son D H 2011 Hot electrons from consecutive exciton-mn energy transfer in Mn-doped semiconductor nanocrystals *J. Phys. Chem.* C **115** 11407–12
[43] Gustafsson M G L, Shao L, Carlton P M, Wang C J R, Golubovskaya I N, Cande W Z, Agard D A and Sedat J W 2008 Three-dimensional resolution doubling in wide-field fluorescence microscopy by structured illumination *Biophys. J.* **94** 4957–70
[44] Lee S F and Osborne M A 2007 Photodynamics of a single quantum dot: fluorescence activation, enhancement, intermittency, and decay *J. Am. Chem. Soc.* **129** 8936–7